

## Georg E. Fantner<sup>1,2</sup>

Postdoctoral Fellow  
Department of Materials Science,  
Massachusetts Institute of Technology,  
Cambridge, MA 02139  
e-mail: fantner@mit.edu

## Daniel J. Burns<sup>2</sup>

Department of Mechanical Engineering,  
Massachusetts Institute of Technology,  
Cambridge, MA 02139  
e-mail: danburns@mit.edu

## Angela M. Belcher

Professor  
Department of Materials Science and Department  
of Biological Engineering,  
Massachusetts Institute of Technology,  
Cambridge, MA 02139  
e-mail: belcher@mit.edu

## Ivo W. Rangelow

Professor  
Department of Micro-Nanoelectrical Systems,  
Technical University Ilmenau,  
Ilmenau 98693, Germany  
e-mail: ivo.rangelow@tu-ilmenau.de

## Kamal Youcef-Toumi

Professor  
Assoc. Mem. ASME  
Department of Mechanical Engineering,  
Massachusetts Institute of Technology,  
Cambridge, MA 02139  
e-mail: youcef@mit.edu

# DMCMN: In Depth Characterization and Control of AFM Cantilevers With Integrated Sensing and Actuation

*New developments in MEMS (microelectromechanical systems) fabrication allowed the development of new types of atomic force microscopy (AFM) sensor with integrated readout circuit and actuator built in on the cantilever. Such a fully instrumented cantilever allows a much more direct measurement and actuation of the cantilever motion and interaction with the sample. This technology is expected to not only allow for high speed imaging but also the miniaturization of AFMs. Based on the complexity of these integrated MEMS devices, a thorough understanding of their behavior and a specialized controls approach is needed to make the most use out of this new technology. In this paper we investigate the intrinsic properties of such MEMS cantilevers and develop a combined approach for sensing and control, optimized for high speed detection and actuation. Further developments based on the results presented in this paper will help to expand the use of atomic force microscopy to a broad range of everyday applications in industrial process control and clinical diagnostics. [DOI: 10.1115/1.4000378]*

## 1 Introduction

Nanotechnology has a profound influence on current research and technology. Almost every field of modern technology and manufacturing utilizes techniques or knowledge gained from nanoscale investigation. In addition to the well known example of semiconductor industry, other industries less associated with small devices (such as metallurgy, chemical engineering, pharmacology, hard disk manufacturers, automotive industry, etc.) use nanotechnology extensively to improve their products. Atomic force microscopy (AFM) has become one of the main tools for nanotechnology, both for characterization as well as manipulation of surfaces. Due to its nondestructive nature and the ability to observe biological samples under ambient conditions, AFM has also become popular in life science and medicine to achieve high resolution images of DNA or tissue. Figure 1 shows a high resolution AFM image of *E. coli* bacteria revealing fine sub features of the cell surface.

One of the main contributions to the success of AFM was the invention of batch fabricated MEMS (microelectromechanical systems) cantilevers by Quate and co-workers [1,2]. The most common method to measure the deflection of these cantilevers uses a laser reflected from the back of the cantilever onto a pho-

todetector. When the cantilever is deflected, the reflected laser beam comes off the cantilever at a different angle. This angle is then amplified by the distance of the cantilever to the sensor and results in a measurable vertical shift of the laser spot on the photodetector. This method is often referred to as *optical lever detection*. Using this basic technique, a wide variety of AFM methods have been invented to measure topography with atomic resolution [3] or single molecules [4], electrical [5], mechanical [6], or magnetic [5] properties.

Although AFM is already widely used in research and high tech industries, AFM in its current form is unsuited for a wide variety of applications, which would benefit from nanoscale characterization and manipulation. Some of these applications are biomedical imaging in hospitals, routine industrial characterization, multiparallel cantilever processing for manufacturing or applications where there is no room for a whole AFM such as in vivo imaging, prefracture crack characterization, or imaging inside a transmission electron microscope (TEM, STEM). Some of the reasons AFM is not suitable for such applications are the size and form of the instruments, the high level of knowledge required to operate the instrument, and the time it takes to acquire an AFM image. The first factor is a sheer size constraint. The optical lever detection method requires optical components, their alignment, and access for alignment. In addition, such optical components take up a large portion of the instrument's physical size. For instance, this is a problem for imaging in a sealed vacuum or cryogenic chamber. For use in clinical settings or routine quality inspection, the complexity and required operator knowledge must be reduced and in vivo imaging of tissue (for instance bone or cartilage [7]) requires

<sup>1</sup>Corresponding author.

<sup>2</sup>GEF and DJB contributed equally to this manuscript.

Contributed by the Dynamic Systems Division of ASME for publication in the JOURNAL OF DYNAMIC SYSTEMS, MEASUREMENT, AND CONTROL. Manuscript received June 22, 2008; final manuscript received June 27, 2009; published online November 6, 2009. Assoc. Editor: J. Karl Hedrick.

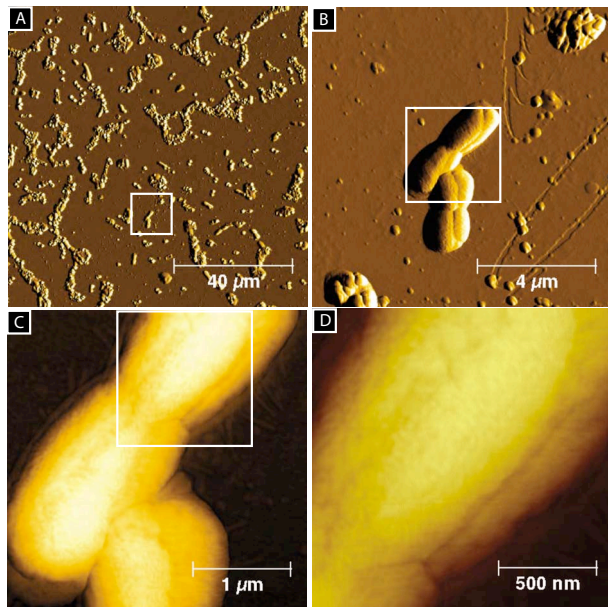


**Fig. 1** AFM images of *E. coli* in tapping mode in air. (a) and (b) are amplitude images. (c) and (d) are phase images for better clarity of the finer features on the cell surface.

small instrument size and ease of use. Innovations in cantilever detection as well as actuation are required to achieve this size reduction.

Soon after the introduction of batch fabricated cantilevers [1,2], new cantilever actuation and detection schemes were developed. The detection schemes include interferometric [8], capacitive [9], thermal [10–12], or piezoresistive [13–17]. In addition to the integrated sensing mechanisms, new actuator types for direct cantilever actuation have been developed such as thermal bimorph actuation [15,18,19], electrostatic [9], electromagnetic [20], or with a piezo film [13,14]. With such sensors and actuators integrated onto the cantilever, the AFM can be made much smaller since the laser and photodetector alignment are no longer necessary. The instrument can be automated to increase usability in nontraditional fields.<sup>3</sup>

Another important limitation of current AFM for use in routine inspection and clinical diagnostics is the long time (2–20 min) it takes to record one image. This speed limitation is due to the mechanical scanning nature of AFM. When scanning faster, mechanical resonances are excited in the scanning system, which distort the image [21]. Also, the speed of the mechanical detection of the topography depends strongly on the resonance frequency and the  $Q$ -factor of the cantilever [22]. The dynamics of the cantilever together with the dynamics of the scanning unit impose a limit on the speed of the feedback loop, which tracks the topography of the sample. The actuator that tracks the topography in the  $z$ -direction needs to be faster than the highest spatial frequency in the imaged sample times the scanning speed. For a conventional piezo tube with a resonance frequency around 2 kHz in the  $z$ -direction and scanning a  $10 \times 10 \mu\text{m}^2$  image at 1 Hz line rate, one cannot record spatial frequencies higher than

<sup>3</sup>We want to point out that these reductions in instrument size are possible with these technologies. For the purpose of this paper, we use an instrument capable of both conventional (laser) detection and piezo actuation to conduct accurate performance comparison. Our system is therefore not smaller nor more automated than a regular AFM system.

$$f_{\text{spatial-max}} \leq v \times f_{\text{res}} = \frac{2 \text{ kHz}}{10 \mu\text{m/s}} = 200 \frac{1}{\mu\text{m}} \quad (1)$$

which corresponds to a surface corrugation with a 5 nm period. At this scan rate, a  $10 \times 10 \mu\text{m}^2$  image with 512 lines takes 8.5 min. In order to reduce the imaging time, it is essential to increase the resonant frequency of the  $z$ -actuator. Since the resonance frequency depends on the mass and stiffness, approaches have been developed to make the actuator support structure stiffer [23] and the actuators smaller [24,25]. Using an actuator directly on the cantilever, one can take advantage of the small size and the high resonance frequency of the actuator [14]. Initially, the actuators were made of piezoelectric material on the back of the cantilevers but required relatively high voltages, which make these cantilevers incompatible with imaging in liquids. An alternative approach to integrate the actuator on the cantilever is to use cantilevers made with layers of materials that have different thermal expansion coefficients and integrate a microheater on the cantilever [15,26,27].

In this paper, we present a detailed investigation into the properties of thermally actuated cantilevers with resistive sensing. We characterize the behavior of the sensing mechanism, the dynamics of the cantilever actuator, as well as the specific control issues that arise from the combination of thermal actuation and piezoresistive sensing. Based on this characterization, we developed a simple controller, which increases the actuation bandwidth of these cantilevers by one order of magnitude. The suitability of such a cantilever for use in AFM imaging with special focus on high speed and routine industrial/clinical applications is discussed.

## 2 Description of Setup and Instrumented Cantilevers

The fabrication and basic characteristics of thermally driven cantilevers with integrated resistive readout has been described in detail previously [15,26]. In brief: we use Si cantilevers  $320 \mu\text{m}$  long,  $110 \mu\text{m}$  wide, and  $3\text{--}5 \mu\text{m}$  thick to investigate the properties of the self sensing and actuation mechanisms. The cantilevers have a piezoresistive element situated on the base of the cantilever and thermal heating loops near the tip. The electrical contacts are made on the cantilever substrate and wire bonded to a printed circuit support chip. There are two contacts for the microheater ( $R \approx 22 \Omega$ ) and two for the piezo resistor ( $R \approx 1 \text{ k}\Omega$ ).

Figure 2 shows the schematic measurement setup. The cantilever is mounted on a custom cantilever holder (with integrated electronics and a piezo stack for exciting the cantilever in resonance) in a MultiMode V AFM (Veeco Metrology, Santa Barbara, CA) and connected to Nanoscope V AFM controller. This configuration allows us to use the cantilevers both in conventional AFM mode as well as using self sensing and self actuating.

## 3 Cantilever Behavior

**3.1 Deflection Sensing.** The deflection of the cantilever can be measured using the piezo resistor on the base of the cantilever. We use the piezo resistor as one leg of a Wheatstone bridge with a 2.048 V precision voltage source as bridge supply. The bridge signal is amplified with an AD8250 instrumentation amplifier (Analog Devices, Norwood, MA) using an optional additional amplification with an external operational amplifier. Figure 3 shows the deflection force curves of the self sensing cantilever measured (a) with the optical lever detection and (b) with the sensing resistor. The gain of the final amplification stage in the resistor readout circuit is adjusted such that the deflection sensitivity of the resistor readout approximately matches the optical deflection sensitivity.<sup>4</sup>

<sup>4</sup>It should be noted here that the optical deflection sensitivity depends strongly on the alignment of the laser on the cantilever. Therefore, the optical deflection sensitivity will be somewhat different each time the laser is readjusted on the cantilever before imaging.

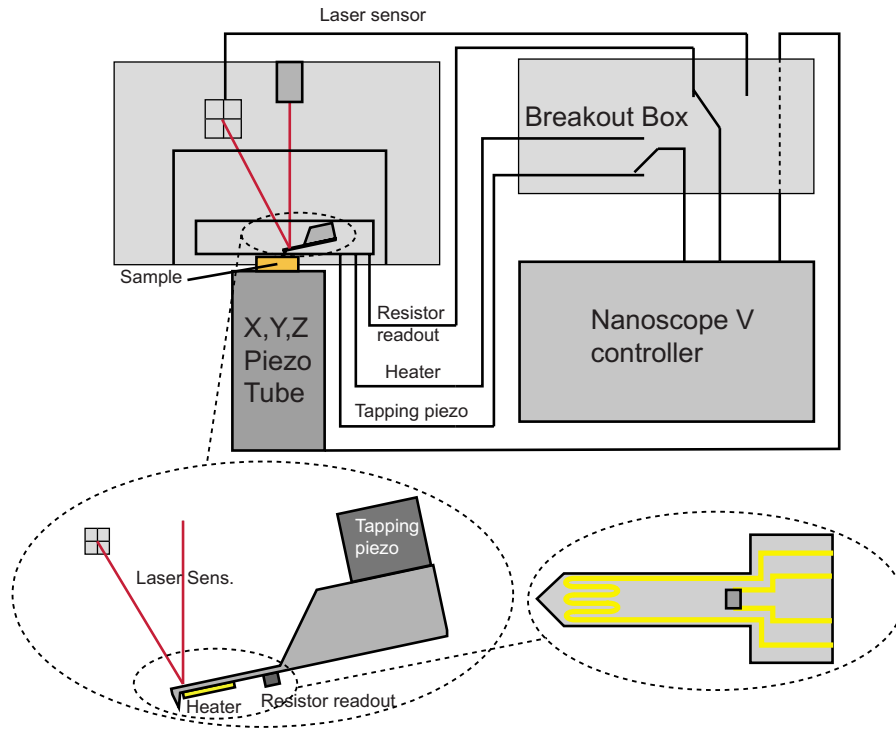


Fig. 2 AFM setup for detection and actuation of instrumented cantilever.

**3.2 Thermal Actuation.** For AFM imaging in tapping mode, it is necessary to excite the cantilever around its resonant frequency as well as control the distance between cantilever and sample to track the topography. Using the actuated cantilevers in a conventional AFM setup allows us to compare the traditional means of cantilever actuation with the new integrated thermal actuator.

The cantilever actuation was done either using the thermal microheater on the cantilever or with standard mechanical actuation using a piezo built into the cantilever holder. The mechanical actuation using the piezo for driving the cantilever in ac-mode has to be used around its resonance to achieve adequate efficiency. The actuator on the cantilever can be used to drive the cantilever in resonance as well as deflect the cantilever at lower frequencies off-resonance. When a dc-voltage is applied to the microheater, the cantilever bends as shown in Fig. 4(a). Since the cantilever deflects with a change in temperature (due to a difference in thermal expansion coefficient), the deflection is proportional to the temperature change  $\Delta T$ , which is proportional to the dissipated electrical power  $P$  in the microheater. The dissipated power in

turn is proportional to the square of the applied voltage ( $P = V^2/R$ ), therefore the cantilever deflection changes quadratically with the input voltage. Figure 4(b) shows the step response of the cantilever from thermal actuator to deflection. The time constant fit to a first-order exponential is  $1503 \text{ s}^{-1}$  and is problematic for tracking topography at high imaging rates. This issue is addressed in Sec. 4.

Actuation around the resonant frequency of the cantilever can be achieved both with the microheater on the cantilever as well as the piezo built into the cantilever holder. Figure 5 shows the frequency response of the cantilever to a sinusoidal sweep; the first and second resonances of the cantilever can be seen clearly.<sup>5</sup>

**3.3 AC Behavior.** To investigate the behavior of the thermal actuation around the resonant frequency, we compare the four combinations of actuation and sensing. Figure 6 shows the cantilever behavior at its first resonance as excited with mechanical (piezo) actuation and thermal (heater) actuation and measured with laser readout and sensing resistor readout, respectively. The curves are recorded using a sinusoidal frequency sweep (Nanoscope V controller, Veeco Metrology). Qualitatively, the spectra of Figs. 6(a)–6(c) show the same behavior with more noise on the traces in case of the sensing resistor readout. Figure 6(d) however shows a less pronounced resonance peak and a phase lead before the resonance. The phase change is also significantly less in magnitude (note the different phase axis in Fig. 6(d)). Since this behavior only occurs when using both the thermal actuation and the resistive sensing, we propose that this is not a physical property of the cantilever but rather an artifact from the measurement. A similar behavior has been reported by Ferrari et al. [28] and Corman et al. [29] for accelerometers and we attribute this behavior to crosstalk between the actuator and the sensor. Three types of

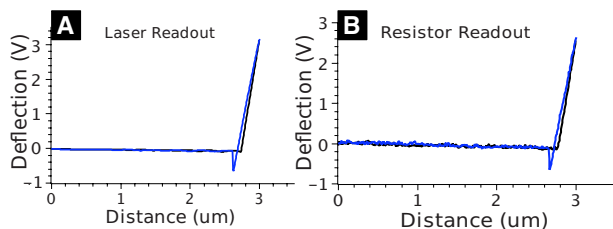
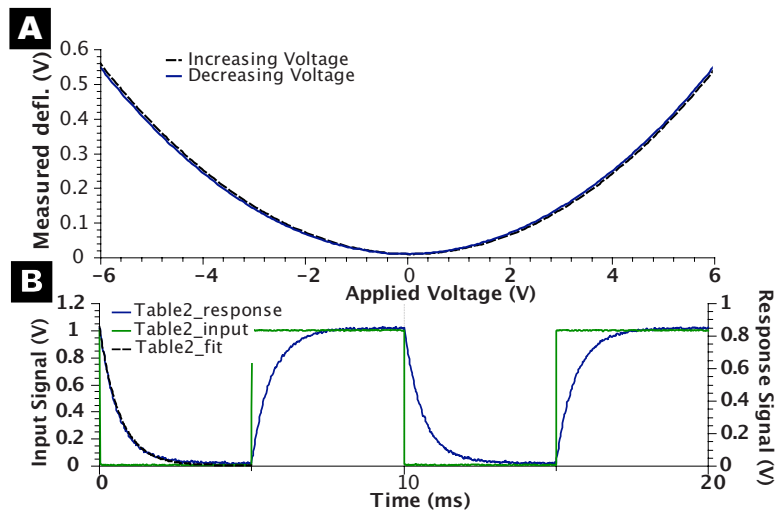


Fig. 3 Contact mode approach curves (a) deflection readout with optical lever deflection. (b) Deflection readout with sensing resistor. The gain of the sensor resistor readout electronics is adjusted to roughly match the deflection sensitivity of the optical lever detection. The graphs are drawn such that the curves have equal height to allow better comparison of curve shape and noise levels.

<sup>5</sup>The large variations in the phase at frequencies not close to the resonances are due to the fact that the amplitude at those frequencies is below the noise floor.



**Fig. 4 Low frequency behavior of cantilever actuator. (a) Deflection of the cantilever for a given applied dc-voltage. (b) Step-response of heater actuation with laser readout.**

crosstalk are possible between the thermal actuator and sensing resistor: capacitive, inductive, and thermal crosstalk. In general, capacitive crosstalk in electronic devices is dominant at higher frequencies, whereas inductive crosstalk is associated with lower frequencies. The thermal crosstalk is strongly dependent on the distance between the thermal actuator and the sensing resistor (in our case it is approximately  $200 \mu\text{m}$ ). We can again divide this crosstalk into a low frequency and a high frequency component.

A low frequency change in overall temperature of the cantilever will result in a mechanical bending of the cantilever due to the bimorph effect [15] as well as a change in the resistance of the sensing resistor due to its thermal coefficient. Both of these effects will change the voltage measured at the output of the Wheatstone

bridge but only the first effect is due to an actual bending of the cantilever. This effect manifests as a shift of the mean value of the sensor signal over time. This is less problematic for tapping mode imaging because the lock-in amplifier removes any offset in the sensor signal. It is, however, still desirable to minimize this effect because a large shift in the mean value can result in saturation of the preamplifiers. Therefore, the cantilever should be oscillated at its resonant frequency for a while before measurements are started to reach a thermal equilibrium.

At higher frequencies (e.g., at the cantilever resonance), the amplitude of the heat pulses that reach the sensing resistor are attenuated significantly [28]. The direct thermal crosstalk (which changes the resistor value due to its thermal coefficient) is negli-

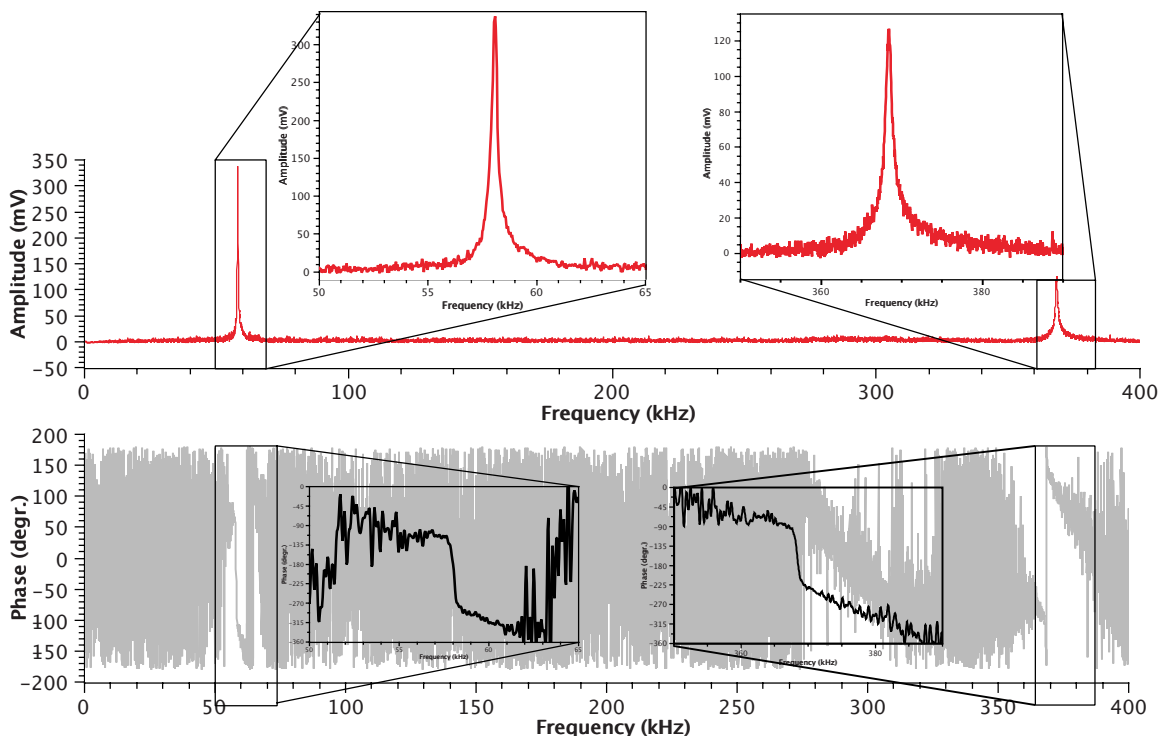


**Fig. 5 Sinusoidal frequency sweep over the first two resonant modes. Excitation with microheater, readout with optical lever detection.**

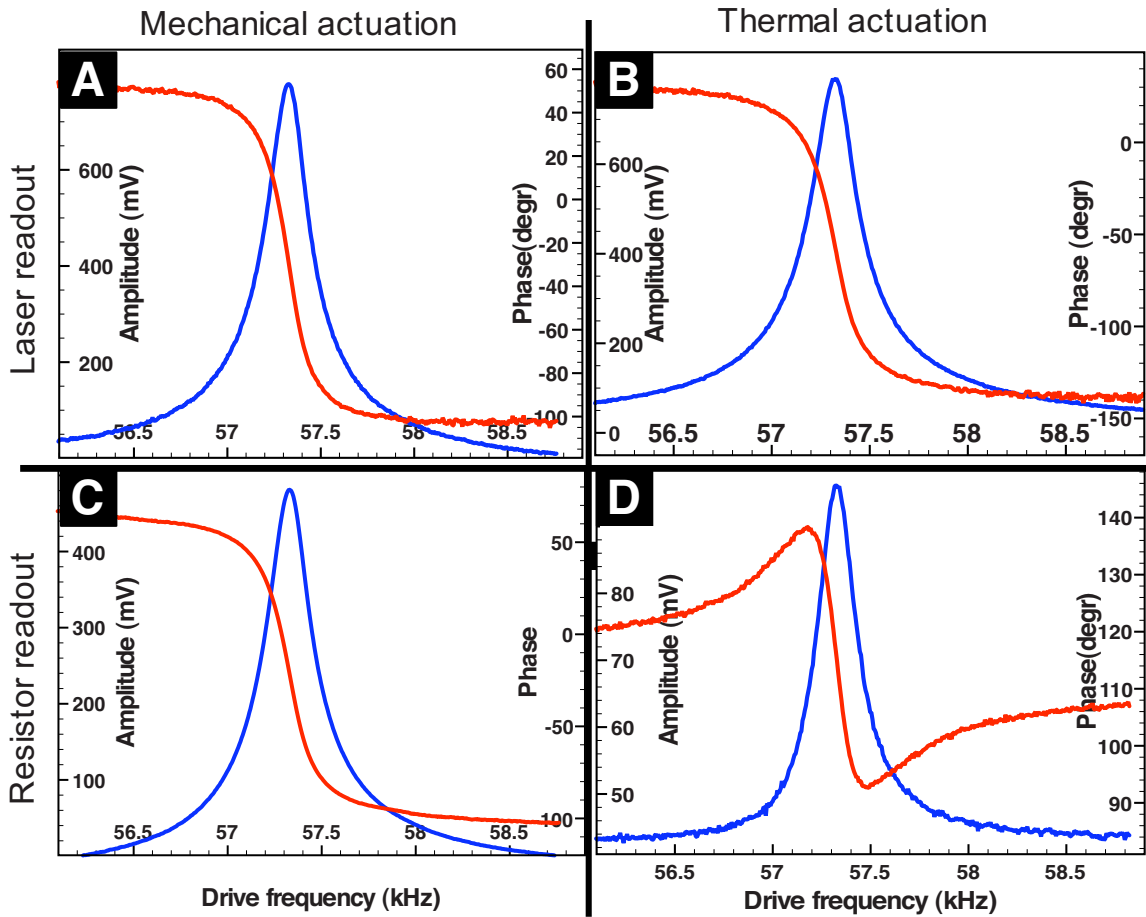


Fig. 6 Swept sine wave tuning curves of active cantilever using optical deflection readout, sensing resistor readout, tapping piezo actuation and heater actuation: (a) optical lever detection and tapping piezo actuation (classical AFM setup), (b) optical lever detection and heater actuation, (c) sensing resistor readout and tapping piezo actuation, and (d) sensing resistor readout and heater actuation.

gible given the distance between the actuator and the sensor. Hence, at high frequencies the thermal influence of the drive signal on the sensor signal is reduced to the actual mechanical bending of the cantilever (as is desired). We propose that the crosstalk between the thermal actuator and the sensing resistor is due to a superposition of the input signal onto the resistor bridge signal (see Fig. 7). We modeled the behavior of the cantilever during the swept sine measurement by simulating the cantilever dynamics with LABVIEW simulation interface toolkit (National Instruments,

Austin, TX). The resulting data are shown in Fig. 8. The individual lines represent simulations with different gains on the crosstalk. With zero gain ( $K=0$ ) in the crosstalk block, the amplitude and the phase behavior is that of a harmonic oscillator. As the crosstalk gain is increased, the starting amplitude shifts up and the phase appears to increase before going down. The entire phase drop becomes less than 180 deg. This behavior is most pronounced in the curves with crosstalk gain at 30 and 40, which appear very similar to the tuning curve in Fig. 6(d) when using the

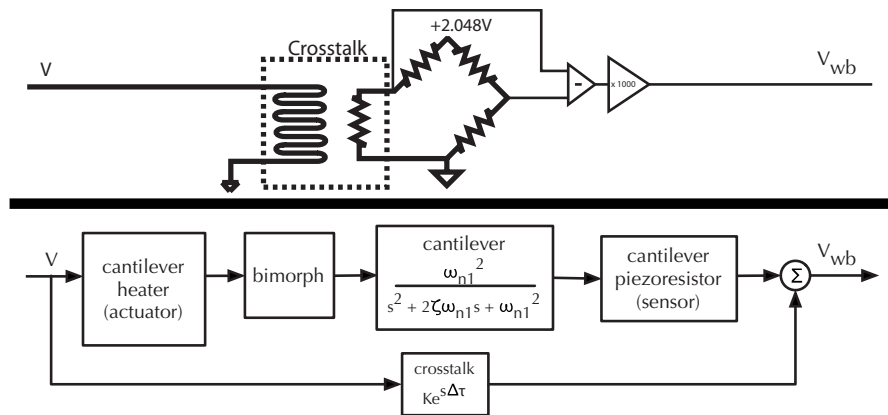
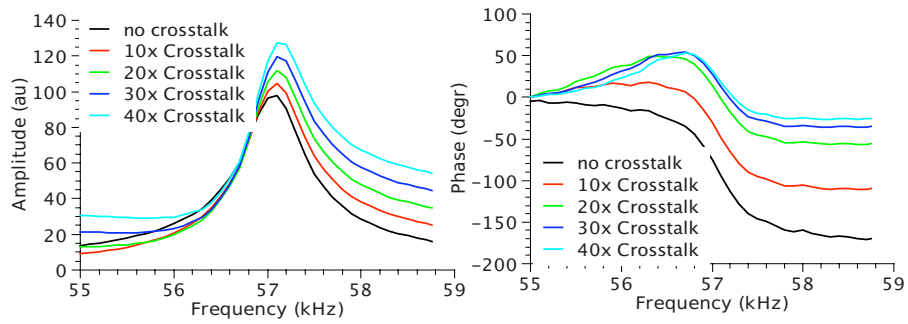
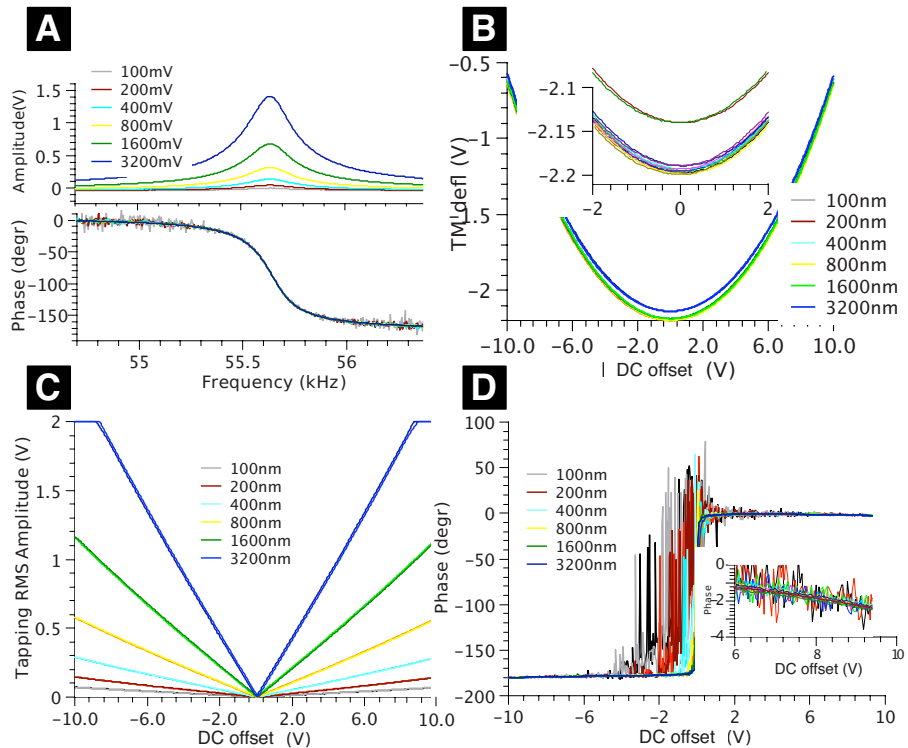


Fig. 7 Connection of thermal actuator and sensing resistor with description of crosstalk between heating signal and resistor sensing signal.



**Fig. 8** Swept sine wave tuning curves of active cantilever using the sensing resistor readout, and heater actuation as modeled with the LABVIEW simulation interface toolkit. The individual traces represent different values of gain for the cross-coupling. Left: amplitude, right: phase. The same simulations at gain 30 and 40 show qualitatively the same behavior as in Fig. 6(d).



**Fig. 9** Influence of dc-offset on ac behavior: (a) Frequency sweep of cantilever measured with laser and driven by thermal actuator at different drive amplitudes (100 mV, 200 mV, 400 mV, 800 mV, 1600 mV, and 3200 mV). (b) Tapping mode deflection as function of dc-offset. The dc-offset is linearly ramped from  $-10$  V to  $+10$  V and the mean value of the oscillating cantilever is measured. (Insert is zoom in around zero dc-voltage). (c) RMS amplitude of oscillating cantilever as function of dc-offset. (d) Phase of cantilever oscillation as function of dc-offset. (Insert shows flat region between 6 V and 10 V).

thermal actuator and the resistor sensor.<sup>6</sup> We therefore conclude that the reduced phase and amplitude transition is an artifact from the measurement. Although it is not necessary for imaging, this measurement error could be compensated electronically to obtain higher sensitivity.

### 3.4 AC-DC Coupling. In regular feedback operation, the

<sup>6</sup>The absolute value of the gain in this simulation does not describe the direct coupling in the actual device because in the simulation we did not take the gain from heater-bimorph-cantilever into account. A crosstalk gain is therefore physically possible.

thermal actuator will be used for both exciting the cantilever in resonance as well as applying the feedback signal for topography. Any coupling between the low frequency and high frequency actuation can result in a distortion of the detection or even instability of the feedback loop. Here we characterize the coupling between the signals at the resonant frequency (we refer to these as the ac signals) and the feedback signals at lower frequency (we refer to these as dc signals). Figure 9 shows the influence of a low frequency signal added to the thermal actuator on the mean value, the amplitude and the phase of the cantilever oscillating in resonance. For this measurement, a triangular wave with amplitude 10

V and frequency 1 Hz was added to the thermal actuator (in addition to the ac drive signal) and the mean value (tapping mode deflection), amplitude, and phase were measured using a digital lock-in amplifier (Nanoscope V). These measurements were repeated with different ac excitation amplitudes (100 mV, 200 mV, 400 mV, 800 mV, 1600 mV, and 3200 mV). Figure 9(a) shows the frequency spectra of an active cantilever driven with thermal actuation at different amplitudes (dc-offset was 5 V, readout with laser). Figure 9(b) shows the expected parabolic behavior of the static deflection on the applied voltage as the deflection is determined by the heat generated according to  $P=V^2/R$ . The tapping mode deflection does not change significantly as the ac amplitude is increased from 100 mV to 1600 mV. Raising the ac amplitude to 3200 mV results in an additional deflection of 0.06 V. This graph shows the inherent nonlinearity of the thermal actuator. Up to 1600 mV drive amplitude, the actuator sensitivity does not change significantly with drive amplitude. At 3200 mV, the deflection shift with drive amplitude manifests as a lower actuator sensitivity which has to be taken into account when measuring absolute topography data.

Figure 9(c) shows the tapping RMS amplitude as a function of dc-offset voltage. The measured amplitude is highly dependent on the dc signal applied to the actuator. In addition, the coupling is dependent on the drive amplitude with a coupling constant between 0.01 for 100 mV drive amplitude and 0.225 for 3200 mV drive amplitude. In most AFM applications, the tapping amplitude is used as a measure for the surface topography and therefore this coupling is problematic. Since the coupling appears linear with dc-voltage, one could counteract this effect in the feedback controller. Another way to feedback on the topography is using the tapping mode phase as the sensor signal. Figure 9(d) shows the change in phase for different offset voltages. The phase curve is the same for all drive amplitudes and only changes strongly around the zero offset value due to noise in the phase detection (because of the low resonance amplitudes at low offset voltages, see Fig. 9(a)). The phase signal above 1 V dc-offset is nearly constant (less than 0.5 deg/V) with respect to the dc-voltage. This makes the phase signal a better choice for feedback than the amplitude with these actuated cantilevers. The disadvantage of feeding back on the phase is that phase signals are often noisier, especially with low driving amplitudes.

We can describe the coupling between the low frequency offset voltage and the oscillation amplitude by calculating the cantilever deflection  $d(t)$  resulting from an applied voltage  $V(t)$ . Since the thermal actuator bends as a result of heating, the deflection ( $d(t)$ ) of the cantilever will be proportional to the power dissipated ( $P(t)$ ).

$$\begin{aligned}
 d(t, \omega) &\propto P(t) \\
 P(t, \omega) &= \frac{V(t)^2}{R} \\
 V(t, \omega) &= A_0 \sin(\omega t) + B \tag{2} \\
 P(t, \omega) &= \frac{A_0^2}{R} \left( \frac{1 - \cos(2\omega t)}{2} \right) + \frac{2A_0 B}{R} \sin(\omega t) + \frac{B^2}{R} \\
 d(t, \omega) &= \frac{1}{R} \left\{ \underbrace{2A_0 B \sin(\omega t)}_{\text{for excitation at } \omega_{n1}} - \underbrace{\frac{A_0^2}{2} \cos(2\omega t)}_{\text{for excitation at } \omega_{n1}/2} \right. \\
 &\quad \left. + \underbrace{\left( B^2 + \frac{A_0^2}{2} \right)}_{\text{for low frequency deflection}} \right\} \otimes h(t)
 \end{aligned}$$

where  $P(t, \omega)$  is the electrical power,  $R$  is the heater resistance,  $\omega$

is the drive frequency,  $h(t)$  is the cantilever impulse response,  $V(t, \omega)$  is the drive voltage,  $A_0$  is the drive amplitude,  $B$  is the dc-offset, and  $d(t, \omega)$  is the cantilever deflection.

This equation describes the four parts of Fig. 9. When driving at the resonant frequency  $\omega$ , only the first term can excite the cantilever resonance. The response of the cantilever resonator scales linearly with  $A_0$ , see Fig. 9(a). This term also scales linearly with the dc-offset of  $B$ , see Fig. 9(c). The tapping mode deflection (term 3 in Eq. (2)) increases parabolically with the dc-offset  $B$  and the drive amplitude  $A_0$ . The phase of the oscillation is determined by the phase of the first term and stays constant except for a 180 deg phase shift at  $B=0$  due to  $A_0^2 B \sin(\omega t) = A_0^2 (-B) \sin(\omega t - \pi)$ . The second term in Eq. (2) shows that the cantilever can also be excited in resonance when driving at half its resonant frequency but with half the efficiency. The advantage, however, is that term 2 is independent of  $B$  so there would be no parasitic influence of the feedback signal onto the tapping amplitude. We can generalize this for any arbitrary signal ( $B(t)$ ) we apply to the heater to track topography

$$\begin{aligned}
 d(t, \omega) &= \frac{1}{R} \left\{ 2A_0 B(t) \sin(\omega t) - \frac{A_0^2}{2} \cos(2\omega t) + \left( B(t)^2 + \frac{A_0^2}{2} \right) \right\} \\
 &\quad \otimes h(t) \tag{3} \\
 &\quad B(t) \cdots \text{topography signal}
 \end{aligned}$$

As long as  $B(t)$  has no spectral components in the vicinity of  $\omega$  or  $\omega/2$ , the applied feedback signal will not disturb the amplitude of the cantilever oscillating at resonance but driven with a voltage of frequency  $\omega/2$  (compare Fig. 10(c) with Fig. 9(c)).

In practical implementation, using either the phase signal for feedback or excite at  $1/2\omega$  will simplify the control scheme significantly. However, most commercial AFM controllers measure the tapping amplitude with a lock-in amplifier around the excitation frequency and will therefore not detect the resonance at  $\omega$  when exciting  $\omega/2$ .

#### 4 Model-Based Thermal Compensation

Active cantilever step responses shown in Fig. 4 demonstrate a response that is too slow to meet the targeted high speed imaging objectives. In order to alleviate this behavior, a compensator is designed from a frequency domain model obtained by system identification techniques.

**4.1 Actuator Dynamics Characterization.** In order to characterize the cantilever dynamics up to (but not including)<sup>7</sup> the first resonant mode with sufficient spectral resolution, a custom system identification program is written for data acquisition and analysis in LABVIEW. A band-limited random binary signal of  $\{0,1\}$   $V$  is applied to the thermal actuator providing a rapid means to gather wide-band frequency data with sufficient spectral resolution (a swept sine approach would yield too much data for tractable processing and subsequent parameterization).

The cantilever deflection  $d(k)$  is recorded with the optical lever sensor and the input signal  $V(k)$  is retained for processing ( $k$  is the discretized time variable corresponding to a sample rate of  $f_s = 200$  kHz). Means are subtracted from the input and output signals to remove dc offsets and facilitate linear system identification. The input autocorrelation  $R_{VV}(\tau)$  and input-output cross-correlation  $R_{Vd}(\tau)$  is computed from

<sup>7</sup>The purpose of this system identification effort is to characterize the cantilever response in the frequency band over which mean deflection will track topographic changes, see Eq. (1), and not to characterize the resonance behavior. Measurements of the resonance modes are provided in Figs. 5 and 6.

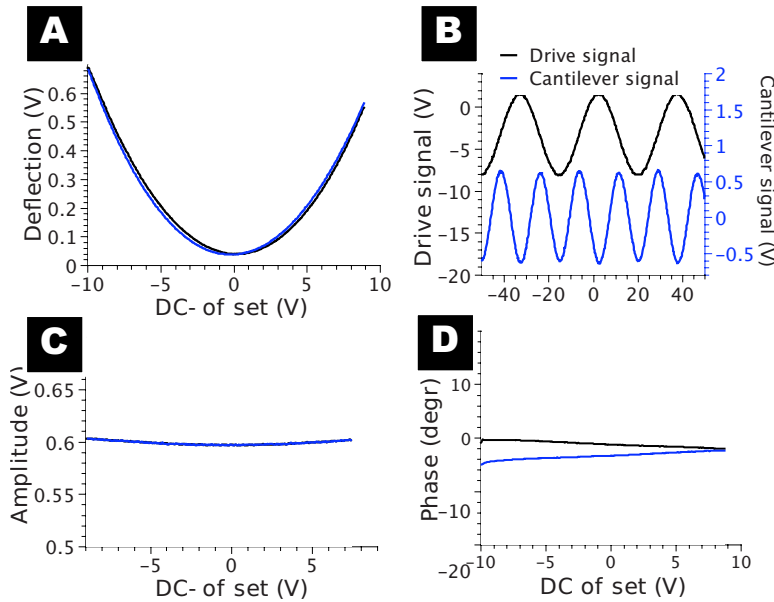


**Fig. 10** Influence of dc-offset on ac behavior when driven at half the resonance frequency: (a) time domain signals—upper trace is excitation and lower trace is response, (b) tapping mode deflection as function of dc-offset—the dc-offset is linearly ramped from  $-10$  V to  $+10$  V and the mean value of the oscillating cantilever is measured, (c) tapping amplitude as function of dc-voltage, and (d) tapping phase as a function of dc-voltage.

$$R_{VV} = \frac{1}{N} \sum_{k=0}^{N-\tau-1} V(k+\tau)V(k)$$

$$R_{Vd} = \frac{1}{N} \sum_{k=\min(\tau,0)}^{N-\max(\tau,0)-1} d(k+\tau)V(k)$$

Note that number of data points available to compute  $R_{VV}$  and  $R_{Vd}$  decreases as the lag  $\tau$  increases causing the correlations to be biased in regions of small signal overlap, and when converted to the frequency domain, causes spectral leakage. To minimize this effect, a Hanning window  $w(\tau)$  is applied such that the weighted correlations approach zero for large lag. Longer window lengths reduce bias because more of the signals overlap. However, a given data record that is divided into fewer, longer windows reduce the number of estimates of  $H(e^{j\omega})$ , which are then averaged together, increasing the variance of the frequency estimation. We found that window lengths of approximately 5% of the sample record balances bias with spectral variance.

The windowed correlations,  $R_{VV}w(\tau)$  and  $R_{Vd}w(\tau)$ , are converted into spectral densities through Fourier transforms,  $\Phi_{VV}$  and  $\Phi_{Vd}$ . The cross-spectral density is divided by the autospectral density to give a nonparametric frequency domain model.

$$H(e^{j\omega}) = \frac{d(e^{j\omega})}{V(e^{j\omega})} = \frac{\Phi_{Vd}(e^{j\omega})}{\Phi_{VV}(e^{j\omega})} \quad (4)$$

This method of finding  $H(e^{j\omega})$  reduces the influence of noise and other effects not associated with the system input-output behavior because it minimizes outputs not correlated with the input [30].

The model obtained in Eq. (4) is parameterized using nonlinear minimization techniques to fit the coefficients of an output-error model. The order of the model is selected using the minimum description length principle [31]. The parameterized model of the active cantilever from thermal actuator voltage to deflection is

$$H(s) = \frac{d(s)}{V(s)} = \frac{1560(s + 95,900)}{(s + 1465)(s + 684,100)} \quad (5)$$

Note that while the gain depends on laser spot alignment, Wheatstone bridge amplification, heater resistance, and other factors, our experience with several cantilevers indicate that the pole and zero locations are repeatable over time. Additionally, we found that these pole and zero locations vary minimally among the different cantilevers tested.

Model validation is performed by comparing the dominant pole determined with system identification techniques at  $1465 \text{ s}^{-1}$  to the time constant fit to the step responses  $1503 \text{ s}^{-1}$  (Fig. 4(b)). This agreement in low frequency behavior indicates that dynamics in this range are dominated by a single pole we attribute to heating and bimorph actuation of the cantilever deflection. Once the cantilever dynamics are satisfactorily modeled, an open-loop filter or *thermal compensator* is designed (see Fig. 12 for a block diagram of the system with thermal compensation).

**4.2 Compensator Design for Increased Bandwidth.** In order to compensate for the relatively slow dynamics identified in Sec. 4.1, and facilitate AFM image reconstruction from scaled controller outputs, an open-loop model-based compensator is used. This open-loop approach is similar to conventional AFM operation in which it is assumed that the  $z$  actuation (typically the piezo tube extension) behaves linearly up to its resonance and reconstructing topography is then an inversion of the actuator's scalar transfer function (i.e., the gain from applied voltage to extension). In order to facilitate AFM image reconstruction from scaled controller outputs, actuator transfer functions should be constant in magnitude over the frequency range of operation. Here, we design the compensator to extend the constant magnitude region of the frequency response to frequencies higher than typical piezo tubes. For the active cantilevers described, actuation bandwidth is targeted at 10 kHz.

A model-based open-loop compensator is designed using loop shaping techniques such that actuator frequency response is flat in

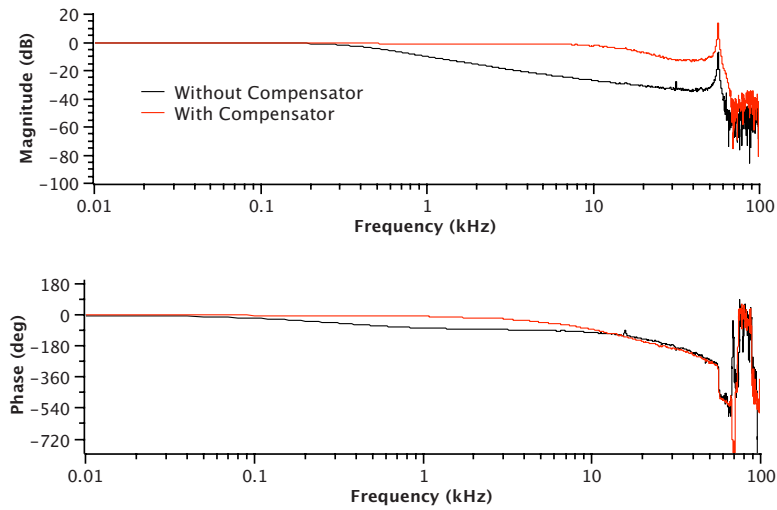


**Fig. 11** Frequency response of the thermally driven cantilever with and without compensation. Deflection is measured with the AFM laser and photodiode. Compensation provides a flat frequency response up to 10 kHz.

magnitude and has minimal phase lag up to the actuation bandwidth. Additional high frequency poles are added for realizability and noise rejection, and the compensator transfer function is discretized using a standard bilinear transformation. The compensator is implemented on an field-programmable gate array (FPGA) at 100 kHz loop rate using the digital filter design toolkit for LABVIEW.

The measured frequency response of the thermal actuator with and without compensation is shown in Fig. 11. The bandwidth of the thermal actuation is increased from approximately 0.4 kHz to 11 kHz, using a 3 dB criterion. This increase in actuator bandwidth observed here is necessary for accurate imaging at reasonable rates. When we tried increasing the actuator response further, we observed unacceptable noise performance and output saturation of the FPGA due to high compensator gain in the passband. Further increases in actuator performance will likely require an inner loop feedback structure where the issue of real time mean cantilever measurement is addressed.

Because our thermal actuator drive electronics conservatively limit cantilever deflection to 750 nm, the piezo tube actuator is required for larger displacements necessary to cover topographic

variation or sample tilt. Therefore, a feedback control strategy that separates controller outputs to two actuators is required and described in the following section.

**4.3 Segmented Control.** In order to take advantage of the thermal actuator's high bandwidth and circumvent its limited range, a segmented control strategy is employed to separate controller outputs. The output of the controller is filtered such that high frequency, low amplitude signals are directed to the thermal actuator and low frequency, large amplitude signals are sent to the piezo tube. In this manner, a single controller can be used, reducing complexity and minimizing the number of free parameters that must be tuned for imaging. Refer to Fig. 12 for a block diagram of the system used for imaging.

To construct an image from the controller outputs, the signals sent to the two actuators ( $V_a$  and  $V_b$  in Fig. 12) must be appropriately scaled and combined. This requires identification of the actuator transfer functions from applied voltage to displacement ( $G_{V_a\delta}$  and  $G_{V_b\delta}$ ). The  $z$  piezo transfer function is easily obtained through standard AFM calibration procedures that typically involve imaging a known standard, providing  $G_{V_a\delta}$ . To obtain  $G_{V_b\delta}$ ,

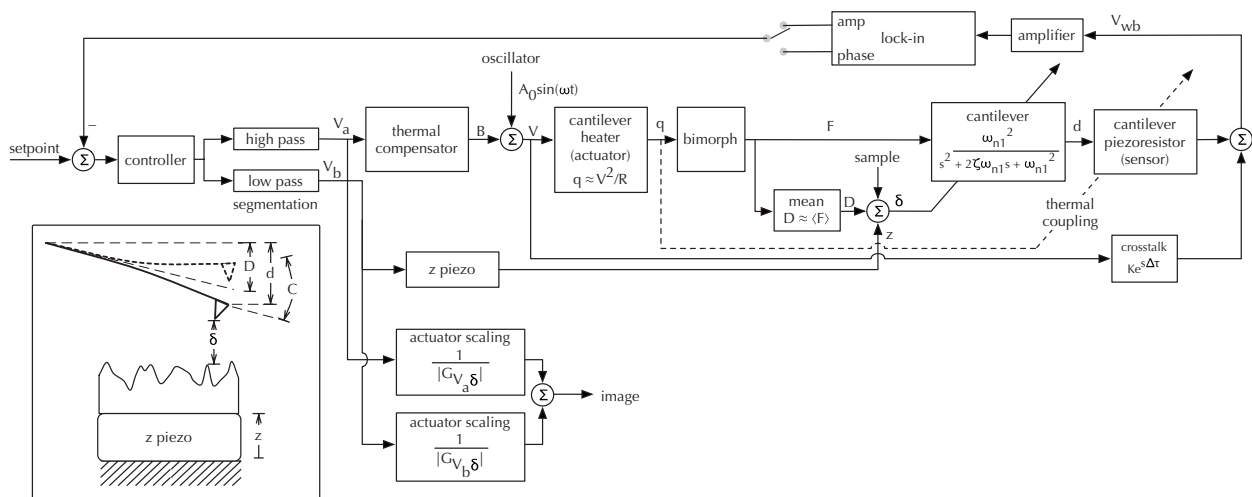


**Fig. 12** Block diagram describing the relationship between all the components

the cantilever is brought in contact with the sample and the piezo is extended by a known amount to calibrate the laser and photodiode. Finally, with the sample retracted, voltage is applied to the thermal actuator  $V_b$  and the mean cantilever deflection is recorded from the photodiode.<sup>8</sup>

More sophisticated dual-input single-output (DISO) control strategies have been extensively developed in hard disk drive head servo systems and may be applicable here [32]. More recently, DISO controllers are being explored in AFM imaging and have demonstrated improvements in imaging speed (see Ref. [33] for a recent review). The method used here is similar to commercially available dual-stage AFM controllers (e.g., Veeco FastScan capability) and is sufficient to demonstrate the principle. Future work will focus on adapting more sophisticated approaches to the present work.

The segmented control approach allows separation of the displacement duties of the imaging system into tasks for which the respective actuators are best suited. In this manner, high frequency commands are processed by the thermal actuator and large displacements are tracked with the piezo tube, and this will ultimately enable higher imaging rates from systems with active cantilevers.

## 5 Discussion

Using actuated and self sensing cantilevers investigated in this paper reveal several aspects that differentiate them from the cantilevers generally used in AFM. The combination of actuation and sensing integrated into one MEMS device without requiring additional hardware such as lasers or piezos allows for the use of AFM in many more areas than conventional AFM. The high integration density of the cantilevers however adds additional aspects that have to be taken into account when using these cantilevers for high quality and high speed AFM applications. Figure 12 shows the block diagram of the system describing the cantilever dynamics, crosstalk, coupling, and feedback schemes. As described in the measurements in Sec. 3 and Fig. 13(a) the cantilevers can be used in regular AFM mode with mechanical tapping actuation and laser readout. In addition, images with good quality can be achieved using any combination of traditional methods and the resistor readout and the thermal tapping actuation (Figs. 13(b)–13(d)). This is consistent with the tuning behaviors of Fig. 6(a)–6(c), which are very similar to each other. Even though the tuning curves in Fig. 6(d) are fundamentally different using both the thermal tapping actuator and the resistive readout showed no significant decrease in image quality on the calibration gratings (see Fig. 13(d)).<sup>9</sup> The  $z$ -feedback actuation in these images is done using the regular piezo tube.

It should be noted here however, that the detection speed of any cantilever in tapping mode is also very much dependent on the dynamics of the cantilever around the resonance frequency [34]. Due to the relative large size (110  $\mu\text{m}$  wide and 320  $\mu\text{m}$  long) and short tip height (3–5  $\mu\text{m}$ ), significant damping of the cantilever oscillation occurs due to displacing the air between the cantilever and the surface. This results in very low  $Q$ -factors of the cantilever oscillation near the surface ( $Q \approx 20$ ) and reduced sensitivity to surface features but increased speed performance (as can be seen in Fig. 14). The increased detection speed is apparent when the scanning speed is stepwise increased from one line per second in Fig. 13(d) to 78 lines per second in Fig. 14. Such high scan speeds are not possible with most conventional cantilevers in tapping mode. However, this increase in detection speed is not

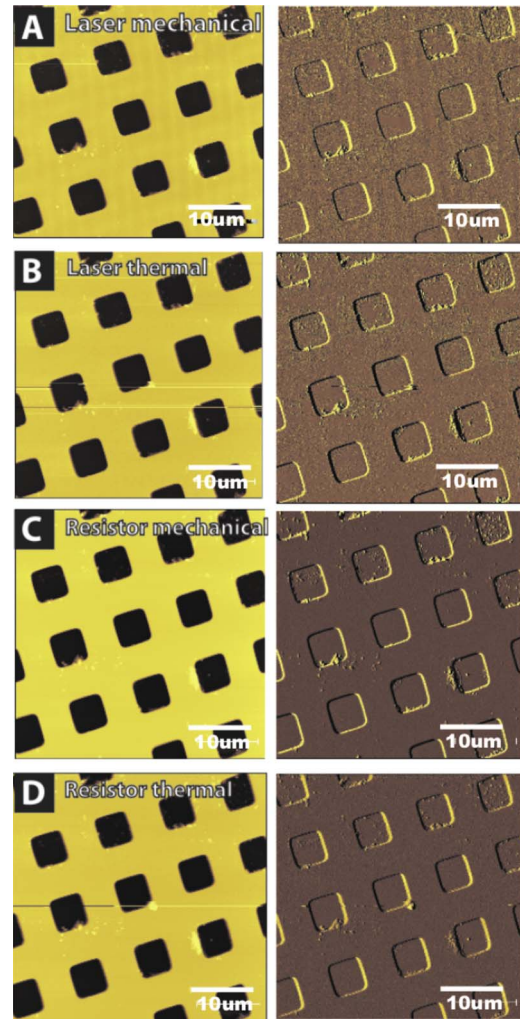


**Fig. 13 Image quality dependent on sensor/actuator combination. (a) sensor: laser, actuator: mechanical (standard AFM configuration, amplitude setpoint is 360 mV). (b) sensor: laser, actuator: thermal (amplitude setpoint is 96 mV). (c) sensor: resistor, actuator: mechanical (amplitude setpoint is 156 mV). (d) sensor: resistor, actuator: thermal (amplitude setpoint is 56.6 mV). The tapping frequency for this cantilever was 56.8 kHz.**

related to the piezoresistive sensing nor the thermal actuation, but rather given due to the dynamics of the cantilever close to the surface. Figure 14(d) shows distortions in the image due to the use of a conventional 130  $\mu\text{m}$  tube scanner for  $x$ ,  $y$ , and  $z$  motion. The distortion is a result of poor  $x, y$  tracking of the piezo tube as well as coupling of the tracking error into the  $z$  motion [35].

Using the integrated thermal actuator for  $z$ -feedback actuation however proved to be less straightforward. In this case, the thermal coupling between the feedback signal applied to the thermal actuator and the actual amplitude with which the cantilever oscillates (see Fig. 9 and the thermal coupling in Fig. 12) results in a more complex situation for approach and feedback control. This effect has been also observed for instrumented accelerometers by Ferrari et al. [28] and Corman et al. [29]. Ferrari et al. [28] propose an active electronic compensation on the piezoresistor signal. Following an equivalent approach in case of the thermally driven AFM cantilevers could be implemented by subtracting a scaled and phase shifted signal to counteract the crosstalk block in Fig. 12 ( $Ke^{s\Delta\tau}$ ). This compensation circuit would have to be tuned for each cantilever (since the coupling is not equally strong due to manufacturing differences). Corman et al. [29] counteract this crosstalk by exciting the accelerometer in *burst*-mode, where they

<sup>8</sup>The mean cantilever deflection  $D = \langle d \rangle$ , changes with applied voltage  $V_b$ , but because the sample is retracted and piezo extension does not influence the cantilever ( $z=0$ ), the transfer function to  $\delta$  is obtained (see Fig. 12).

<sup>9</sup>We use a calibration grating to have a standardized sample to compare the performance with other measurements. However a sample with smaller topography might show more differences in the behavior using the different actuation and sensing schemes.

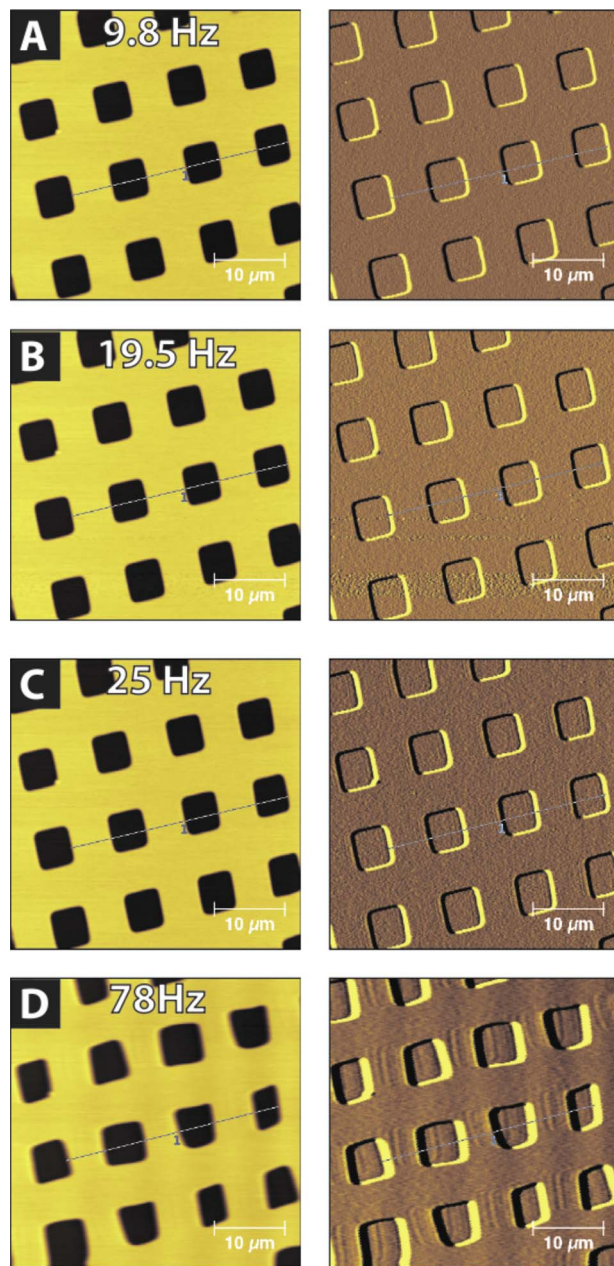


**Fig. 14** Quality of AFM image in tapping mode at different scan speeds. (a) 9.8 Hz linerate, (b) 19.5 Hz linerate, (c) 25 Hz linerate, and (d) 78 Hz linerate. For this measurement, we have used the bridge resistor for detection and the regular piezo scanner for feedback. The cantilever was excited using inertial drive at 57 kHz with an amplitude setpoint of 600 mV.

switch between excitation and detection sequentially. It would be more difficult to adapt this method for use in AFM applications, since this requires a relatively high  $Q$  oscillator and increases the required detection time.

In addition, we only use 750 nm of thermal actuation (of the 2–3  $\mu\text{m}$  predicted to be possible) due to a fixed current limit added in series with the thermal actuator to prevent it from burning up. This makes imaging samples with larger topography variations with only the actuated cantilever impossible. To circumvent this problem, the segmented control scheme described in Sec. 4.3 is used, whereby the thermally driven cantilever is used to track sample topography, and oscillated near resonance with the piezo integrated into the cantilever holder. This should be distinguished from other experiments discussed earlier in this section where

control is performed over the  $z$  piezo only and the cantilever oscillated thermally or with the integrated cantilever holder piezo. For the large changes in topography, we use a conventional piezo tube for very low frequency tracking of the sample topography. For this purpose, the feedback signal coming from the proportional-integral-differential controller is low-pass filtered at as low as 10 mHz and applied to the scanner (the segmentation part in Fig. 12).

A 4  $\mu\text{m}$  scan of a 1  $\mu\text{m}$ -pitch silicon grating is imaged at 4 Hz line rate and scan lines from the image are shown in Fig. 15 with a section of the image inset. The image is created by linearly combining the outputs of the high-pass and low-pass filters, scaled by the inverse of the actuator transfer function gains (see Fig. 12). With the thermal compensator in the loop, controller gains are tuned to provide the best tracking (and further increased slightly to induce borderline oscillatory behavior). The upper two-thirds of the inset figure is taken with the compensator in the loop then the compensator is bypassed, resulting in large amplitude oscillations and destabilizing the feedback loop. This illustrates the stability improvement of the closed loop system under thermal actuator compensation due to increased phase margin shown in Fig. 11.

Examining scan lines with and without the thermal compensator demonstrates that the uncompensated actuator with the lower phase margin causes the feedback loop to destabilize with large amplitude oscillations at  $f_1=175$  Hz, while the compensated actuator shows only minor ringing beginning  $f_2=524$  Hz.

As shown in Fig. 10, the problem with coupling between the lower frequency feedback signal and the tapping amplitude signal can be circumvented by exiting the cantilever with a signal at half of its resonant frequency. A higher driving amplitude is necessary to excite the cantilever in this mode than when driving directly at the resonant frequency, this corresponds well with the derived formula in Eq. (2). However, we were not able to test this mode of operation during imaging due to limitations in our AFM controller. An additional lock-in amplifier, which locks in on double the drive frequency would be required for feedback in this mode. An alternative is to excite the cantilever at its resonant frequency and perform the feedback over the phase rather than the amplitude, which is a common feature in most recent AFM controllers.

## 6 Conclusions

In this paper, we have investigated fully actuated and self sensing cantilevers for their mechanical and electrical characteristics as well as their controllability use in tapping mode atomic force microscopy. We found that the cantilevers can be successfully used for high resolution and high speed imaging, however several issues have to be taken into account to utilize the cantilevers full potential. One such issue is the crosstalk of the tapping drive signal and the deflection signal measured with the integrated resistor, which distorts the measured amplitude and frequency response used for topography feedback. This crosstalk can be minimized by feeding back on the tapping phase signal or by compensating electronically. When using the integrated actuator for feedback actuation as well as tapping actuation, the amplitude of the resulting cantilever oscillation depends linearly on the applied feedback signal. We have identified two ways to prevent this from generating distortions in the image or instabilities of the feedback loop: exciting the cantilever oscillation with a sine signal at half the resonant frequency of the cantilever or feeding back on the tapping phase rather than the tapping amplitude. Using a frequency dependent compensator we were able to increase the actuation bandwidth of the cantilever from 0.4 kHz to 11 kHz, which is essential for high speed AFM imaging. The achievable cantilever deflection was enough to image samples with low topography variations but for samples with large height changes, a second, slow actuator extends the range significantly without impairing speed performance. Overall, we have shown that the self sensing and self actuated cantilevers are very promising for extending the capabilities of AFM in terms of imaging speed and

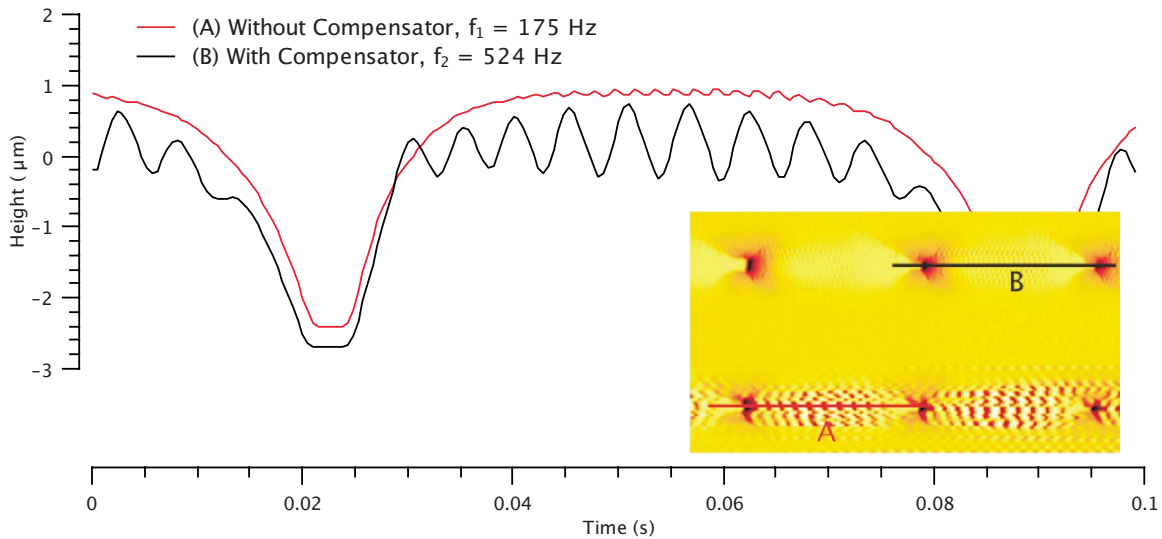


**Fig. 15** Scan lines taken during imaging demonstrate increased stability of the thermal actuator under compensation. For the same imaging parameters (controller gains, scan speed, etc.) the frequency of parasitic oscillation is increased from 175 Hz to 524 Hz and the amplitude is dramatically reduced, indicating better closed-loop stability margins. Inset: AFM image from which the scan lines are taken.

increased usability. We expect this technology to help transform AFM from a tool used in research setting or high tech industry to use in everyday quality control and clinical diagnostics.

### Acknowledgment

The authors would like to thank the support of the Singapore-MIT Alliance. This work was supported by the army research office Institute for Collaborative Biotechnologies, the National Institute of Health under Award No. RO1 GM65354, by the NASA University Research, Engineering and Technology Institute on Bio-Inspired Materials under Award No. NCC-1-02037 and by the Austrian Research Promotion Agency under award number V0156-08-BII: NSI-FABICAN. GEF thanks the Schrödinger foundation for fellowship support.

### References

- [1] Akamine, S., Barrett, R. C., and Quate, C. F., 1990, "Improved Atomic Force Microscope Images Using Microcantilevers With Sharp Tips," *Appl. Phys. Lett.*, **57**(3), pp. 316–318.
- [2] Albrecht, T. R., Akamine, S., Carver, T. E., and Quate, C. F., 1990, "Micro-fabrication of Cantilever Styli for the Atomic Force Microscope," *J. Vac. Sci. Technol. A*, **8**(4), pp. 3386–3396.
- [3] Marti, O., Drake, B., and Hansma, P. K., 1987, "Atomic Force Microscopy of Liquid-Covered Surfaces—Atomic Resolution Images," *Appl. Phys. Lett.*, **51**(7), pp. 484–486.
- [4] Fritz, M., Radmacher, M., Cleveland, J. P., Allersma, M. W., Stewart, R. J., Gieselmann, R., Janmey, P., Schmidt, C. F., and Hansma, P. K., 1995, "Imaging Globular and Filamentous Proteins in Physiological Buffer Solutions With Tapping Mode Atomic-Force Microscopy," *Langmuir*, **11**(9), pp. 3529–3535.
- [5] Martin, Y., Abraham, D. W., and Wickramasinghe, H. K., 1988, "High-Resolution Capacitance Measurement and Potentiometry by Force Microscopy," *Appl. Phys. Lett.*, **52**(13), pp. 1103–1105.
- [6] Vanderwerf, K. O., Putman, C. A. J., Degrooth, B. G., and Greve, J., 1994, "Adhesion Force Imaging in Air and Liquid by Adhesion Mode Atomic-Force Microscopy," *Appl. Phys. Lett.*, **65**(9), pp. 1195–1197.
- [7] Imer, R., Akiyama, T., De Rooij, N. F., Stolz, M., Aebi, U., Friederich, N. F., Koenig, U., Wirz, D., Daniels, A. U., and Stauffer, U., 2006, "Development of Atomic Force Microscope for Arthroscopic Knee Cartilage Inspection," *Jpn. J. Appl. Phys., Part 1*, **45**(3B), pp. 2319–2323.
- [8] Ruf, A., Abraham, M., Diebel, J., Ehrfeld, W., Guthner, P., Lacher, M., Mayr, K., and Reinhardt, J., 1997, "Integrated Fabry-Perot Distance Control for Atomic Force Microscopy," *J. Vac. Sci. Technol. B*, **15**(3), pp. 579–585.
- [9] Brugger, J., Blanc, N., Renaud, P., and Derooji, N. F., 1994, "Microlever With Combined Integrated Sensor Actuator Functions for Scanning Force Microscopy," *Sens. Actuators A*, **43**(1–3), pp. 339–345.
- [10] Lee, J., Beechem, T., Wright, T. L., Nelson, B. A., Graham, S., and King, W. P., 2006, "Electrical, Thermal, and Mechanical Characterization of Silicon Microcantilever Heaters," *J. Microelectromech. Syst.*, **15**(6), pp. 1644–1655.
- [11] Lee, J., and King, W. P., 2008, "Improved All-Silicon Microcantilever Heaters With Integrated Piezoresistive Sensing," *J. Microelectromech. Syst.*, **17**(2), pp. 432–445.
- [12] Lee, J., and King, W. P., 2008, "Liquid Operation of Silicon Microcantilever Heaters," *IEEE Sens. J.*, **8**(11), pp. 1805–1806.
- [13] Minne, S. C., Manalis, S. R., and Quate, C. F., 1995, "Parallel Atomic Force Microscopy Using Cantilevers With Integrated Piezoresistive Sensors and Integrated Piezoelectric Actuators," *Appl. Phys. Lett.*, **67**(26), pp. 3918–3920.
- [14] Manalis, S. R., Minne, S. C., and Quate, C. F., 1996, "Atomic Force Microscopy for High Speed Imaging Using Cantilevers With an Integrated Actuator and Sensor," *Appl. Phys. Lett.*, **68**(6), pp. 871–873.
- [15] Ivanov, T., Gotszalk, T., Grabiec, P., Tomerov, E., and Rangelow, I., 2003, "Thermally Driven Micromechanical Beam With Piezoresistive Deflection Readout," *Microelectron. Eng.*, **67–68**, pp. 550–556.
- [16] Ivanov, T., Gotszalk, T., Sulzbach, T., Chakarov, I., and Rangelow, I., 2003, "AFM Cantilever With Ultrathin Transistor-Channel Piezoresistor: Quantum Confinement," *Microelectron. Eng.*, **67–68**, pp. 534–541.
- [17] Linnemann, R., Gotszalk, T., Hadjiiski, L., and Rangelow, I. W., 1995, "Characterization of a Cantilever With an Integrated Deflection Sensor," *Thin Solid Films*, **264**(2), pp. 159–164.
- [18] Hillier, A. C., and Bard, A. J., 1997, "AC-Mode Atomic Force Microscope Imaging in Air and Solutions With a Thermally Driven Bimetallic Cantilever Probe," *Rev. Sci. Instrum.*, **68**(5), pp. 2082–2090.
- [19] Marti, O., Ruf, A., Hipp, M., Bielefeldt, H., Colchero, J., and Mlynek, J., 1992, "Mechanical and Thermal Effects of Laser Irradiation on Force Microscope Cantilevers," *Ultramicroscopy*, **42–44**, pp. 345–350.
- [20] Malo, J., and Izpura, J. I., 2007, "Simultaneous Magnetic and Electrostatic Driving of Microcantilevers," *Sens. Actuators A*, **136**(1), pp. 347–357.
- [21] Schitter, G., Stark, R. W., and Stemmer, A., 2004, "Fast Contact-Mode Atomic Force Microscopy on Biological Specimen by Model-Based Control," *Ultramicroscopy*, **100**(3–4), pp. 253–257.
- [22] Butt, H. J., Siedle, P., Seifert, K., Fendler, K., Seeger, T., Bamberg, E., Weisenhorn, A. L., Goldie, K., and Engel, A., 1993, "Scan Speed Limit in Atomic Force Microscopy," *J. Microsc.-Oxford*, **169**, pp. 75–84.
- [23] Fantner, G. E., Schitter, G., Kindt, J. H., Ivanov, T., Ivanova, K., Patel, R., Holten-Andersen, N., Adams, J., Thurner, P. J., Rangelow, I. W., and Hansma, P. K., 2006, "Components for High Speed Atomic Force Microscopy," *Ultramicroscopy*, **106**(8–9), pp. 881–887.
- [24] Ando, T., Kodera, N., Takai, E., Maruyama, D., Saito, K., and Toda, A., 2001, "A High-Speed Atomic Force Microscope for Studying Biological Macromolecules," *Proc. Natl. Acad. Sci. U.S.A.*, **98**(22), pp. 12468–12472.
- [25] Kindt, J. H., Fantner, G. E., Cutroni, J. A., and Hansma, P. K., 2004, "Rigid Design of Fast Scanning Probe Microscopes Using Finite Element Analysis," *Ultramicroscopy*, **100**(3–4), pp. 259–265.
- [26] Pedrak, R., Ivanov, T., Ivanova, K., Gotszalk, T., Abedinov, N., Rangelow, I., Edinger, K., Tomerov, E., Schenkel, T., and Hudek, P., 2003, "Micromachined Atomic Force Microscopy Sensor With Integrated Piezoresistive, Sensor and Thermal Bimorph Actuator for High-Speed Tapping-Mode Atomic Force Microscopy Phase-Imaging in Higher Eigenmodes," *J. Vac. Sci. Technol. B*, **21**(6), pp. 3102–3107.
- [27] Lee, J., and King, W. P., 2007, "Microcantilever Actuation Via Periodic Internal Heating," *Rev. Sci. Instrum.*, **78**(12), p. 126102.
- [28] Ferrari, V., Ghisla, A., Marioli, D., and Taroni, A., 2005, "Silicon Resonant Accelerometer With Electronic Compensation of Input-Output Cross-Talk," *Sens. Actuators A*, **123–124**, pp. 258–266.

- [29] Corman, T., Noren, K., Enoksson, P., Melin, J., and Stemme, G., 2000, "'Burst' Technology With Feedback-Loop Control Forcapacitive Detection and Electrostatic Excitation," *Electron Devices*, **47**, pp. 2228–2235.
- [30] Ljung, L., 1999, *System Identification: Theory for the User*, Prentice–Hall, Englewood Cliffs, NJ.
- [31] Rissanen, J., 1986, "Stochastic Complexity and Modeling," *Ann. Stat.*, **14**, pp. 1080–1100.
- [32] Kobayashi, M., and Horowitz, R., 2001, "Track Seek Control for Hard Disk Dual-Stage Servo Systems," *IEEE Trans. Magn.*, **37**(2), pp. 949–954.
- [33] Devasia, S., Eleftheriou, E., and Moheimani, S., 2007, "A Survey of Control Issues in Nanopositioning," *IEEE Trans. Control Syst. Technol.*, **15**(5), pp. 802–823.
- [34] Kokavecz, J., Marti, O., Heszler, P., and Mechler, A., 2006, "Imaging Bandwidth of the Tapping Mode Atomic Force Microscope Probe," *Phys. Rev. B*, **73**(15), p. 155403.
- [35] Zou, Q., Leang, K., Sadoun, E., Reed, M., and Devasia, S., 2004, "Control Issues in High-Speed AFM for Biological Applications: Collagen Imaging Example," *Asian J. Control*, **6**(2), pp. 164–178.